Journal of Electronic Research and Application, 2024, Volume 8, Issue 4
http://ojs.bbwpublisher.com/index.php/JERA
ISSN Online: 2208-3510
ISSN Print: 2208-3502

Analysis of Aluminum Alloy Double-Pulse MIG Welding Arc Signal Characteristics Based on Broadband Mode Decomposition

Yin Si[1], Zixiong Xia[2], Wei Liu[1], Kexin Zhang[1], Xiangyu Song[1]*

[1]School of Information and Intelligent Engineering, Guangzhou Xinhua University, Guangzhou 510000, Guangdong Province, China
[2]School of Mechanical and Electrical Engineering, Guangdong Engineering Polytechnic, Qingyuan 511510, Guangdong Province, China

***Corresponding author:** Xiangyu Song, sxyfighting@163.com

Abstract: Welding voltage and current in arc signals are directly related to arc stability and welding quality. Process experiments with different parameters were organized according to the orthogonal experimental design method by constructing an aluminum alloy double-pulse metal inert gas (MIG) welding arc electric signal test platform. The data acquisition system of the aluminum alloy MIG welding process was established to obtain real-time arc signal information reflecting the welding process. The aluminum alloy's collected double-pulse arc current signals are decomposed adaptively by broadband mode decomposition (BMD). The direct current (DC) signal, pulse signal, distortion signal, ripple signal, and noise signal are separated and extracted, and the composite multiscale fuzzy entropy (CMFE) is calculated for the component set of the electrical signal. The experimental results show that the current waveform obtained by the double-pulse MIG welding current signal is consistent with the corresponding weld forming diagram. Simultaneously, the composite multiscale fuzzy entropy is calculated for the arc characteristic parameters. The rationality of matching process parameters and arc stability of aluminum alloy's double-pulse MIG welding were evaluated.

Keywords: Double-pulse MIG welding; Electric arc signal; Broadband mode decomposition; Welding stability

Online publication: August 13, 2024

1. Introduction

Aluminum alloy is used in MIG welding despite the process being prone to oxidation, cracking, and bubble formation, as well as welding deformation and other defects. Additionally, the complexity of the welding equipment, the difficulty in adjusting process parameters, and the lack of quality control measures contribute to the challenges. Any slight deviation in production conditions during the welding process makes it difficult to ensure the consistent quality of the weld [1-3]. To ensure the forming quality of aluminum alloy MIG welding, it is necessary to monitor the quality information of the process and its influencing factors [4-6]. In mechanical engineering, the adaptive time-frequency analysis method for signals has always been a hot research topic [7-9]. In recent years, adaptive time-

frequency analysis has been widely used to extract effective features from complex non-stationary signals disturbed by noise. Common methods include empirical mode decomposition (EMD), ensemble empirical mode decomposition (EEMD), variational mode decomposition (VMD), and so on. Broadband mode decomposition (BMD) is a new adaptive time-frequency analysis method [10]. The BMD method begins by establishing a joint dictionary of wideband effective signals (such as square waves and sharp waves) along with local narrowband signals. An intelligent optimization algorithm is used to search for the sparsest solution of the signal within this constructed dictionary. BMD utilizes a regularization smoothness operator as its optimization objective function, targeting the parameters such as the amplitude, frequency, and phase of the wideband effective signals, as well as the filter parameters of the local narrowband signals. Through the use of intelligent optimization algorithms, BMD achieves sparse signal decomposition during the optimization process. Compared with the previous adaptive time-frequency analysis method, the BMD method can separate the "sharp angle" wideband effective signal and local narrowband signal from the complex non-stationary signal, and realize the feature extraction of the effective mode in the wide band range.

In this paper, the direct characteristic information of arc signal during aluminum alloy double-pulse MIG welding is analyzed through the electric arc signal test experiment. The collected arc current signal is decomposed by BMD, and the distortion components of the current waveform with different frequencies are obtained. On this basis, the composite multiscale fuzzy entropy calculation (CMFE) is carried out, which provides a new experimental method and reference for the stability analysis of arc signal and welding quality evaluation of the aluminum alloy double-pulse MIG welding process.

2. Test platform

To study the characteristics of electric arc signals during welding, the experimental platform for electric arc signal testing of aluminum alloy double-pulse MIG welding in the process can not only accurately and conveniently collect electric arc signals online, but also detect and analyze arc stability and weld forming quality. This paper introduces in detail the experimental setup for aluminum alloy MIG welding and arc electric signal testing, focusing on aluminum alloy double-pulse MIG welding as the experimental subject.

2.1. The overall composition of the experimental platform

The aluminum alloy double-pulse MIG welding experiment and arc electric signal test platform setup are shown in **Figure 1**. The test platform comprises a double-pulse metal inert gas (DPMIG-500) welding machine, welding robot, wire feeding mechanism, argon tank, and arc signal data acquisition system. The experiment involves using the DPMIG-500 welding machine and welding robot for a double-pulse MIG welding surfacing experiment. The workpiece material is 6061 aluminum alloy with dimensions of 250 mm × 200 mm × 5 mm. The welding parameters include an argon flow rate of 10 L/min, dry extension of welding wire 15 mm, welding wire model ER5356, and welding wire diameter of φ1.2mm. The specific functions of each component are shown in **Table 1**.

The aluminum alloy MIG welding arc electric signal data acquisition system includes current and voltage sensors, data acquisition cards, and computers for storing and analyzing data. Through the MIG welding system, the welding current and voltage, the welding speed and the start and stop functions of the welding machine can be set respectively. The welding current and voltage signals are sent to the collection box through the hall current sensor and the electrical isolation voltage sensor is arranged in the transmission box. After processing by the acquisition system, it is transmitted to the computer by ethernet interface for oscilloscope and storage. The sampling frequency is 12 kHz, sampling 25 s per welding process, 24,000 data points were intercepted for

BMD decomposition and frequency analysis.

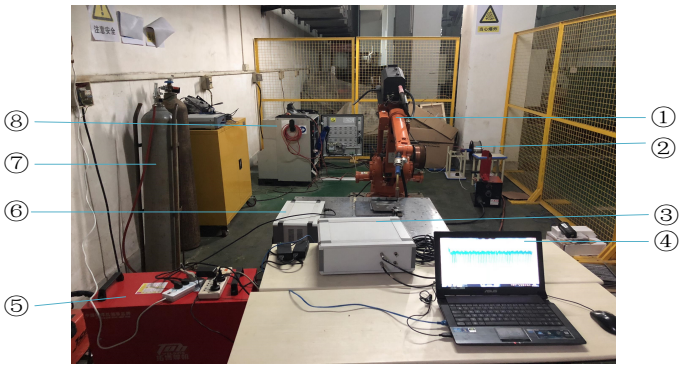

Figure 1. MIG welding experiment and test platform with (1) welding robot (2) wire feeder (3) arc signal data acquisition box (4) computer (5) welding machine (6) arc sensor box (7) argon gas storage tank 8) power supply

Table 1. Main components and functions of the experimental platform

Item	Function
DPMIG-500 aluminum welding machine	Responsible for setting welding process parameters such as welding peak voltage, welding base value voltage, welding peak current, welding base value current, duty cycle, welding frequency, and starting and stopping welding experiments.
ABB IRB1410 Industrial Robot	Control welding speed and other sizes and travel direction.
Data acquisition system	Including a sensor box, acquisition box, computer, and communication cable. For high speed and accurate storage of welding arc data.
Wire feeder	Includes wire feed tray and wire feed controller. Manual wire feeding and automatic wire feeding are available for choice.
Argon gas storage tank	Inert gas argon is provided while the wire is transported. To isolate air outside the welding area and prevent oxidation.

2.2. Double-pulse MIG welding process experiment

At different welding process parameters, the welding current signal collected synchronously during the welding process is transmitted to the industrial computer for display and storage. The collected signals are analyzed and processed with the help of MATLAB software with specific data points extracted from the DP-MIG welding current signal for detailed analysis. The welding parameters are shown in **Table 2**.

Table 2. DP-MIG process parameters

Experimental sequence number	Welding speed (mm/s)	Spike current (A)	Base current (A)	Spike voltage (V)	Base voltage (V)	Duty ratio (%)	impulse frequency (Hz)
1	1	50	40	21	17.5	50	2
2	1.5	50	40	21	17.5	50	2
3	5	50	40	21	17.5	50	2
4	5	60	40	21	17.5	50	5

Four sets of different welding process parameters were selected for double-pulse MIG welding to analyze their respective effectiveness and welding process stability. The appearance of weld formations from each experimental group is depicted in **Figure 2** respectively. **Figure 3** shows the waveform diagram of the DP-MIG welding current signal.

As shown in **Figure 2**, there is a biting phenomenon at the tail of the weld surface of experiment No. 1. The weld surface of experiment No. 3 has obvious welding defects such as lack of penetration, lack of fusion, and poor surface forming. Weld surfaces of experiments No. 2 and No. 4 formed well.

The appearance of weld No. 1 is shown in **Figure 3(a)**. Initially, the weld exhibited a uniform fish scale pattern, indicating overall good formation. However, towards the end of the weld, there was some edging observed. The weld surface appeared angular, irregular, and slightly sunken. Analysis of the intercepted 2 s welding arc current signal revealed the following: In the low-frequency pulse phase, welding commenced with automatic wire feeding, forming an arc that joined the molten pool. The arc's impact caused the coarse crystals in the molten pool to break up, achieving grain refinement. As the welding frequency in the low-frequency pulse group increased, further stirring occurred inside the molten pool, refining the weld grain. The corresponding welding arc current signal is sparse. In the high-frequency pulse group phase, the welding wire melted, and droplets formed and transitioned into the molten pool. The corresponding welding arc signal showed periodic transformation.

The appearance of weld No. 2 is presented in **Figure 3(b)**. The whole weld showed a uniform and regular fish scale pattern, but the spacing between the fish scale pattern is larger than that of weld No. 1. Analysis of the intercepted 2 s welding arc current signal revealed that in the low-frequency pulse phase, welding slowly started to arc with automatic wire feeding where the arc joins the molten pool. The impact of the arc caused the coarse crystals in the molten pool to break up to achieve the effect of grain refinement. The increase of welding frequency in the low-frequency pulse phase further stirred the inside of the weld pool, refining the weld grain and the corresponding welding arc current signal showed sparse phenomenon. In the high-frequency pulse phase, the welding wire melted and droplets slowly formed and transitioned into the molten pool. The corresponding welding arc signal presents a periodic change, but the stirring time is too long in the initial formation of the molten pool, so the distance between the figure of the fish scale pattern is large.

The appearance of weld No. 3 is shown in **Figure 3(c)**. There are obvious welding defects such as lack of penetration, lack of fusion, and poor surface forming on the surface of the whole weld. Analysis of the intercepted 2 s welding arc current signal presented that in the low-frequency pulse phase, the welding current signal is first dense and then sparse. In the high-frequency pulse phase, the current distribution is relatively uniform and dense. Thus, in a single cycle, the molten pool is formed in the low pulse group and with a large size. However, in the high pulse group, the transition density of molten drops is too large and concentrated together to form the welding hump defect. In the double-pulse MIG welding cycle of about 1.1 s and 1.5 s, the welding seam has an obvious arc-breaking phenomenon in the current waveform, hence the weld surface forms defects.

The appearance of weld No. 4 is shown in **Figure 3(d)**. The whole weld shows a uniform and regular fish scale pattern. However, the spacing between the fish scale pattern is larger than that of weld No. 1 and No. 2. Analysis of the intercepted 2 s welding arc current signal showed that in the low-frequency pulse phase, welding begins to arc slowly with automatic wire feeding where the arc joins the molten pool. The impact of the arc causes the coarse crystals in the molten pool to break up, achieving grain refinement. The welding frequency in the low-frequency pulse group increased to further stir the inside of the molten pool, refining the weld grain. The corresponding welding arc current signal is sparse. In the high-frequency pulse phase, the welding wire is melted and the molten droplets are slowly formed and transferred into the molten pool. The corresponding welding arc signal presents a periodic transformation. However, the stirring time is short at the initial stage of molten pool formation, thus the spacing between the figure of fish scales is larger.

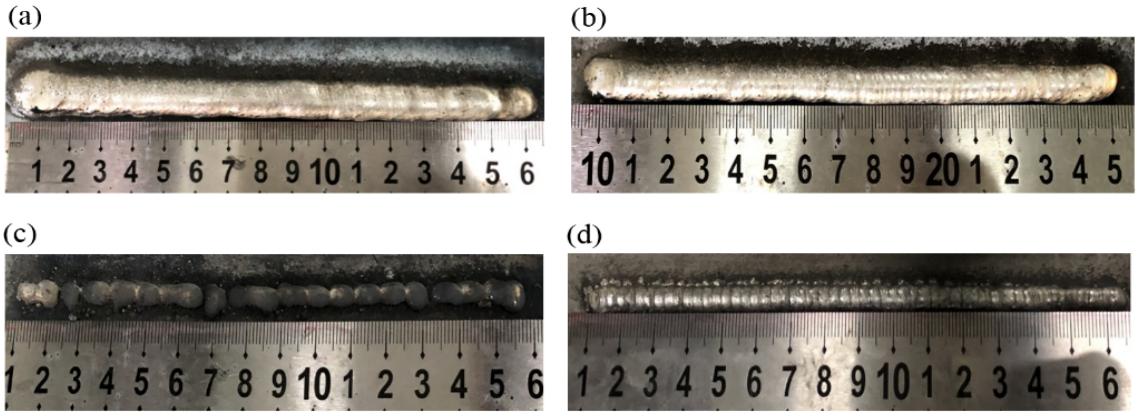

Figure 2. DP-MIG weld appearance molding

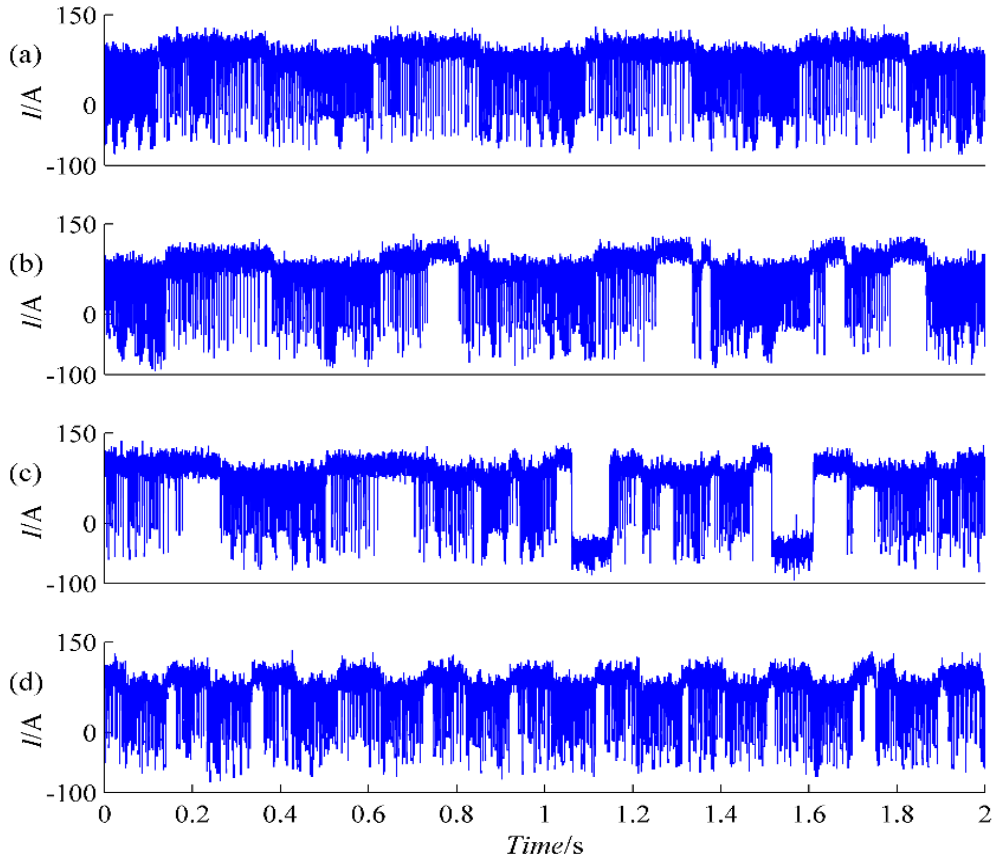

Figure 3. Waveform of DP-MIG welding current signal

3. Processing and analysis of experimental results

3.1. Welding arc signal decomposition based on BMD

BMD can effectively separate wideband signals such as square waves, sharp waves, and narrow band signals composed of sine waves from the complex non-stationary direct current signal.

For signals$x(n)$, the iterative process of the BMD method is as follows:

(1) Command $r_0(n)=x(n)$.

(2) Filter out the DC component of the signal, intrinsic mode function (IMF): $IMF_0(n)=IFFT[r_0(1)]$, where $r_0(1)$ is the first component obtained by the Fourier transform of $r_0(n)$, and command $r_1(n)=x(n)-IMF_0(n)$.

(3) Command i=1, the following constrained optimization problem P1 is established:

$$P1: Minimize \quad T_1(A_1,\omega_1,\theta_1,D_1),T_2(A_2,\omega_2,\theta_2,D_2),T_3[A_3(n),\omega_3,\theta_3(n)] \tag{1}$$

$$S.T.\ x(n)=\sum_{i=0}^{N} IMF_i(n)+res(n),\ \theta_i\in[0,\ 2\pi],\ D_i\in[0,\ 1]$$

therein:

$$T_{j(j=1,2)}=\left\|D^{(2)}\left[IMF_i^j(n)\right]\right\|_2^2+\lambda\left\|D^{(2)}\left[x(n)-IMF_i^j(n)\right]\right\|_2^2 \tag{2}$$

$$IMF_i^1(n)=A_1 square(\omega_1 n+\theta_1,D_1) \tag{3}$$

$$IMF_i^2(n)=A_2 sawtooch(\omega_2 n+\theta_2,D_2) \tag{4}$$

$$IMF_i^3(n)=A_3(n)\cos[\omega_3+\theta_3(n)] \tag{5}$$

(4) The optimization problem P1 is solved by the ACROA algorithm, to get the best $T_{j(j=1,2,3)}$, then find the smallest number with T_1, T_2 and T_3, $T_{j(best)}$, command $IMF_i(n)=IMF_i^{j(best)}(n)$ [11].

(5) Command $r_{i+1}(n)=r_i(n)-IMF_i(n)$.

(6) Determine whether the decomposition results meet the iteration termination condition $\frac{\left\|IMF_i(n)-IMF_{i-1}(n)\right\|_2^2}{\left\|IMF_{i-1}(n)\right\|_2^2}\le\varepsilon$, if yes, end the iteration process and set i=i+1, if not, return to step (3).

IMF1 and IMF2 obtained by current signal decomposition using the BMD method are shown in **Figure 4**. The BMD effectively separates the square wave components from the signal, the peak-to-peak value and pulse frequency of IMF1 obtained by decomposition are consistent with the peak-to-peak value of the square wave current signal set in **Table 2**. The decomposed IMF2 retained the nonlinear information and distortion information related to weld quality. **Figure 5** shows the instantaneous amplitude (IA) and instantaneous frequency (IF) of IMF2 obtained by the decomposition of 2 s signal intercepted in experiments No. 1–4.

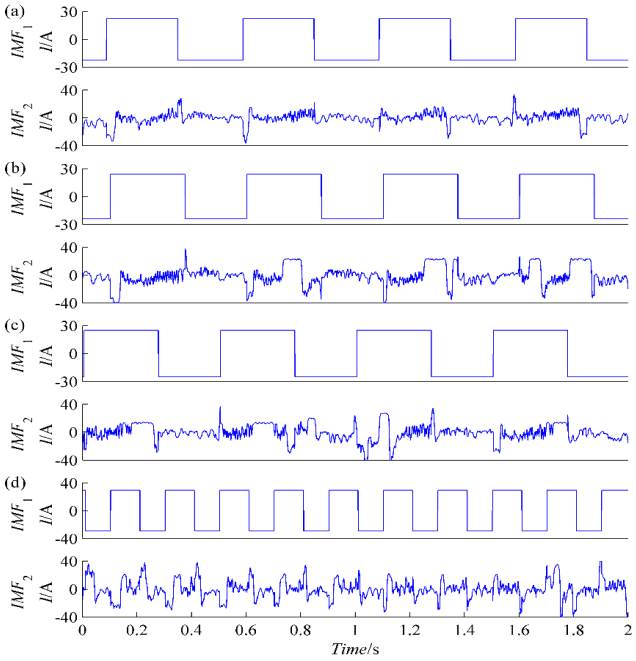

Figure 4. IMF1 and IMF2 obtained by BMD decomposition of current signals, (a)–(d) are the decomposition results of the interception 2 s of experiments No. 1–4

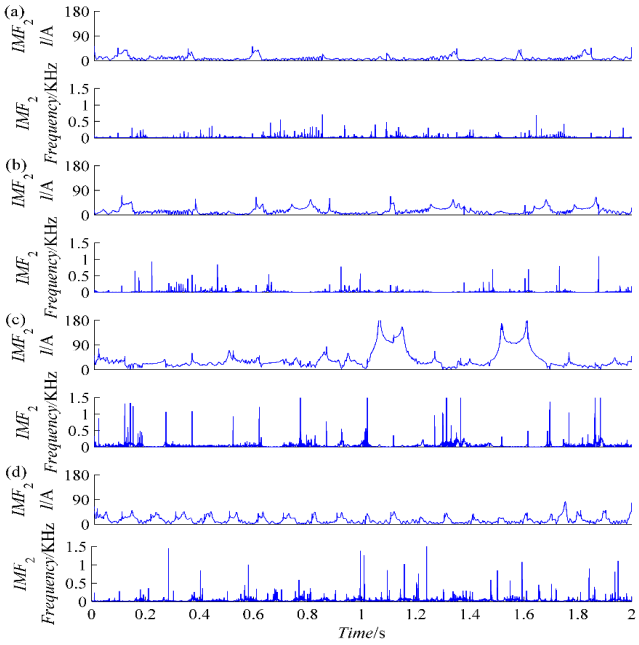

Figure 5. Time-frequency analysis of current signal BMD decomposition results (a)–(d) are the IA and IF of IMF2 components obtained by 2 s decomposition of experiments No. 1–4 current signal interception

Experiments No. 1, 2, and 3 showed consistent duty cycle and pulse frequencies in the welding current signal, each conducted at varying welding speeds. **Figure 5(c)** illustrates noticeable instantaneous amplitude changes in the time-domain waveform of the current during experiment No. 3. This is caused by the arc-breaking phenomenon due to poor welding quality. The time-frequency distributions in **Figure 5(a)–(c)** reveal that with increased welding speed, arc energy rises, leading to a significant increase in frequency component. Experiments No. 3 and 4 explored welding current signals under identical welding speed and duty cycle conditions, but with different pulse frequencies. In experiment No. 4, the time-frequency information of the IMF2 component from the intercepted signal appears more stable. This is because the arc energy in the welding process is more concentrated at higher pulse frequencies, resulting in better welding quality.

3.2. Calculation and analysis of characteristic parameters of aluminum alloy double-pulse MIG welding signal

After the signal decomposition using the BMD method, it is necessary to select a suitable eigenvalue to evaluate the effective component of the electrical signal. In this paper, the compound multiscale fuzzy entropy (CMFE) recently proposed by Jin *et al* is used to evaluate the power quality of welding inverters at different welding speeds and pulse frequencies [12].

In the CMFE algorithm, to address the impact of shorter time series on fuzzy entropy calculation in during coarse-graining, the mean fuzzy entropy value of different coarse-grained sequences with the same scale factor is used as the fuzzy entropy value for that scale factor [13].

CMFE calculation steps are as follows:

(1) For time series $\{x(i), i = 1, 2, \cdots, N\}$, define different coarse-grained sequences $y_k^{(\tau)} = \left\{ y_{k,1}^{(\tau)}\ y_{k,2}^{(\tau)} \cdots y_{k,p}^{(\tau)} \right\}$, mean:

$$y_{k,j}^{(\tau)} = \frac{1}{\tau} \sum_{i=(j-1)\tau+k}^{j\tau+k-1} x_i,\ 1 \le j \le N/\tau, 1 \le k \le \tau \tag{6}$$

(2) For each scale factor τ, the fuzzy entropy of each coarse-grain sequence $y_k^{(\tau)} (1 \le k \le \tau)$ is calculated,

then to average τ entropy, CMFE at this scale factor is obtained:

$$CMFE(X,\tau,m,n,r)=\frac{1}{\tau}\sum_{k=1}^{\tau}FuzzyEn(y_k^{(\tau)},m,n,r) \tag{7}$$

CMFE synthesizes the fuzzy entropy information of all coarse-grained sequences at the same scale. CMFE curves reflect the complexity of time series under different scale factors. For a direct current signal, the greater the calculated fuzzy entropy, the more ambiguous it is, the less stable the data, and the worse its power quality. Conversely, the lower the fuzzy entropy, the less ambiguous it is, the more stable the data, the better the power quality. The welding current signals collected in each experiment were divided into 25 groups of data at equal intervals. The duration of each set of data is 1 s, the composite multi-scale fuzzy entropy is calculated ($\tau=2$). The calculation results are shown in **Figure 6**, and the average value of composite multiscale fuzzy entropy for each group of experiments is shown in **Table 3**.

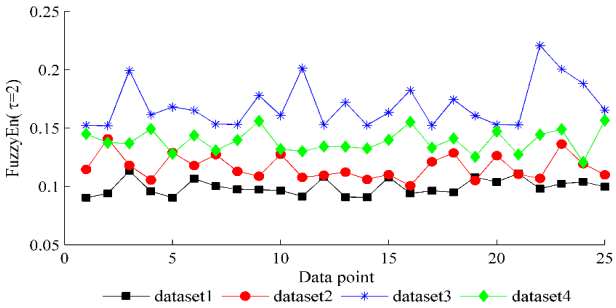

Figure 6. Composite multiscale fuzzy entropy of IMF2 component obtained from BMD decomposition of experiments No. 1–4 current signal

Table 3. The average composite multiscale fuzzy entropy of each group of experiments

Experiment number	1	2	3	4
Calculated entropy	0.0993	0.1166	0.1694	0.1388

As seen from **Table 2** and **Table 3**, the compound multi-scale fuzzy entropy increases with the increase of welding speed. This is because as the welding speed increases, the arc stability in the welding process relatively decreases, making the degree of electrical energy dispersion increase, and causing arc breakage. Thus the composite multiscale fuzzy entropy of the corresponding welding current signal increases. The weld in experiment No. 3 has an obvious arc breakage in the current waveform as it is easy to arc during the welding process, hence the entropy value is large.

At the same welding speed, duty cycle, and welding voltage, among other factors, different frequencies exhibit reduced complexity in multiscale fuzzy entropy calculation. This indicates the arc is more stable. This stability arises because, with increased frequency, the welding speed matches the frequency, leading to periodic alignment of the welding waveform. This concentrates the arc energy during the welding process, resulting in a corresponding decrease in composite multiscale fuzzy entropy of the welding current signal.

4. Conclusion

(1) In aluminum alloy double-pulse MIG welding speed, a change in frequency will result in a different distribution of arc energy in the time and frequency domains, and thus the stability of welding arc and weld forming quality are affected. Therefore, by reasonable matching of aluminum alloy MIG welding

current waveform parameters, it can effectively obtain a uniform distribution of arc energy in the time domain and frequency domain. This ensures the stability of the welding process and obtains good welding results.

(2) The BMD method is a new adaptive decomposition method suitable for the processing of non-stationary signals. Through the aluminum alloy double-pulse MIG welding arc electric signal test, real-time arc signal information reflecting the welding process was obtained. The BMD method was applied to extract the characteristic information of the electric arc signal. It can effectively separate different frequency DC components, pulsed square wave current, and current signal distortion components of double-pulse MIG welding. The composite multiscale fuzzy entropy is used to calculate the distortion component. The results showed that the BMD method combined with composite multiscale fuzzy entropy can effectively evaluate the signal quality of the welding inverter.

Funding

The 2024 University-level Higher Education Teaching Reform Project of Guangzhou Xinhua University, "Teaching Reform and Practice Based on OBE Concept: A Case Study of "University Physics Experiment" (Project No. 2024J044)

Disclosure statement

The authors declare no conflict of interest.

Author contributions

Conceptualization: Yin Si
Investigation: Yin Si, Zixiong Xia
Formal analysis: Wei Liu, Kexin Zhang, Xiangyu Song
Writing: Wei Liu, Kexin Zhang, Xiangyu Song

References

[1] Basheer UM, Noor AFM, Zuhailawati H, et al., 2013, Advances in friction welding process: A review. Science and Technology of Welding and Joining, 15(7): 534–558.

[2] Kimapong K, Watanabe T, 2005, Effect of Welding Process Parameters on Mechanical Property of FSW Lap Joint between Aluminum Alloy and Steel. Materials Transactions, 46(10): 2211–2217.

[3] Karthikeyan R, Balasubramanian V, 2012, Optimisation and sensitivity analysis of friction stir spot-welding process parameters for joining AA 6061 aluminum alloy. International Journal of Manufacturing Research, 7(3): 257–272.

[4] Li Y, Zhao Y, Zhou X, et al., 2021, Effect of Droplet Transition on the Dynamic Behavior of the Keyhole during 6061 Aluminum Alloy Laser-MIG Hybrid Welding. The International Journal of Advanced Manufacturing Technology, 119: 897–909. https://doi.org/10.1007/s00170-021-08270-1

[5] Wang JB, Nishimura H, Katayama S, et al., 2008, Study of Laser-MIG Hybrid Welding of Aluminum Alloy. Preprints of the National Meeting of JWS, 2008: 105. https://doi.org/10.14920/jwstaikai.2008s.0.5.0

[6] Wang Y, Wei B, Guo Y, et al., 2017, Microstructure and mechanical properties of the joint of 6061 aluminum alloy by plasma-MIG hybrid welding. China Welding (English Edition), 26(002): 58–64.

[7] Czerwinski RN, Jones DL, 1995, Adaptive cone-kernel time-frequency analysis. Signal Processing IEEE Transactions on Signal Processing, 43(7): 1715–1719.

[8] Hou TY, Shi Z, 2011, Adaptive Data Analysis via Sparse Time-Frequency Representation. Advances in Adaptive Data Analysis, 3(1–2): 1–28. http://dx.doi.org/10.1142/S1793536911000647

[9] Wang XK, Gao JH, He YY, 2010, Time-frequency analysis based on time-frequency-adaptive optimal-kernel. Systems Engineering and Electronics, 32(1): 22–26.

[10] Enghardt L, Moreau A, Tapken U, et al., 2013, Radial Mode Decomposition in the Outlet of a LP Turbine–Estimation of the Relative Importance of Broadband Noise. Journal of Health Communication, 19(4): 392–412.

[11] Alatas B, 2011, ACROA: Artificial Chemical Reaction Optimization Algorithm for global optimization. Expert Systems with Applications, 38(10): 13170–13180.

[12] Jin Z, Xiao Y, He D, et al., 2023, Fault diagnosis of bearing based on refined piecewise composite multivariate multiscale fuzzy entropy. Digital Signal Processing, 2023: 133.

[13] Zheng J, Pan H, Cheng J, 2017, Rolling bearing fault detection and diagnosis based on composite multiscale fuzzy entropy and ensemble support vector machines. Mechanical Systems and Signal Processing, 85: 746–759.